Journal of Alloys and Compounds 495 (2010) 453–457

Contents lists available at ScienceDirect

Journal of Alloys and Compounds

journal homepage: www.elsevier.com/locate/jallcom

Structural analysis of platinum–palladium nanoparticles dispersed on titanium dioxide to evaluate cyclo-olefines reactivity

N. Castillo[a,e,*], R. Pérez[b], M.J. Martínez-Ortiz[c], L. Díaz-Barriga[c], L. García[d], A. Conde-Gallardo[e]

[a] Facultad de Química, Universidad Nacional Autónoma de México, Edificio B, 04510 México DF, Mexico
[b] Instituto de Ciencias Físicas, Universidad Nacional Autónoma de México, Campus Morelos, 62251 Cuernavaca Morelos, Mexico
[c] Instituto Politécnico Nacional - ESIQIE, UPALM Edif. 7, 07738 México DF, Mexico
[d] Instituto Politécnico Nacional - ESIT, UPALM, 07738 México DF, Mexico
[e] Centro de Investigación y de Estudios Avanzados del IPN, Depto. de Física, Av. IPN 2508, C.P. 07360, México DF, Mexico

ARTICLE INFO

Article history:
Received 11 July 2008
Received in revised form
21 November 2009
Accepted 24 November 2009
Available online 1 December 2009

Keywords:
Nanoparticles Pd–Pt
TEM
XRD

ABSTRACT

Structural and chemical properties were correlated to explain catalytic behavior of Pt–Pd/TiO_2 in a cyclo-olefin reaction. Bimetallic nanoparticles supported on TiO_2 were prepared by wetness impregnation techniques at different concentrations of Pt and Pd ≈1 metallic wt%. The physicochemical properties of these metallic nanoparticles supported on TiO_2 were characterized by N_2 physisorption (Brunauer–Emmett–Teller—BET), X-ray diffraction (XRD), and transmission electron microscopy (TEM). The relationship between chemical composition, physicochemical properties and particle size on the cyclo-olefin reaction was then studied.

XRD and TEM results show that these nanoparticles are composed of Pt–Pd with FFC structure (a = 0.389–0.391 nm) supported on TiO_2 (anatase-like structure), and the materials present tetragonal structure nanoparticles (a = 0.37842, b = 0.37842, c = 0.95146 nm). Samples with higher contents of platinum and particle sizes of 4.2 nm show the highest catalytic conversion in cyclo-olefins reaction. Finally, structural examinations of Pt_x–$Pd_{(1-x)}$/TiO_2 based system was then conducted to study the effects of metals on the nanostructure of the materials.

1. Introduction

Several studies have attracted the importance of isomerization reactions in naphtha reforming and olefins to increase octane number using heterogeneous catalysis using supported metals as catalysts [1]. Therefore, during the last decade various methods for producing bimetallic materials have been developed and they have proved to be very efficient in different chemical reactions. This kind of material is used for the reduction of gaseous pollutants from the environment incorporating noble metals in to different supports. Particularly, platinum and palladium can be used in a wide range of reactions.

In this context, titanium dioxide anatase-like structure is a favorable support for Pt-based catalysts because of its good surface properties and resistance to poisoning. TiO_2 is one of the most useful materials for environmental cleaning, catalysis, gas sensing, batteries, and solar cells [2,3]. In addition, platinum and palladium are used in several catalytic reactions as hydrogenation, dehydrogenation and isomerization.

Specifically, Pt–Pd bimetallic systems have been used in unsaturated hydrocarbons hydrogenation reactions: hydrogenation of unsaturated hydrocarbons and aromatics [4–7], hydrogenation of o-chloroaniline to chloronitrobenzene, tetraline in the presence of hydrogen sulfide [8–11], since these systems are highly resistant to poisoning by sulfur and nitrogen. It is also important to note the high activity on hydrogenation reactions. They have also been used for oxidation reactions, such as SO_2 to SO_3 [1], formic acid electro-oxidation [12,13], methanol oxidation and combustion [14,15], hydrodesulfurization of 4,6-dimethyldibenzothiofene and dibenzothiofene [16] and the synthesis of H_2O_2 [17]. A variety of oxides have been used as supports of platinum and palladium metallic particles: SiO_2 [17,18], SiO_2/Al_2O_3 [19], C [20], Al_2O_3 [21], PS [22,23], γ-Al_2O_3 [24,25], zeolites [18,26–28], Al_2O_3 [29,30], SiO_2–Al_2O_3 [31], and Al_2O_3–B_2O_3 [32]. Although, in many cases, the composition of bimetallic nanoparticles is different from those of macroscopic alloys, and the combination of different properties in nanoparticles depends upon the combination and distribution of atoms in the alloy [33,34]. Particularly, the interest in Pt–Pd bimetallic supported catalysts in hydrocarbons reactions has been initiated by both, practical and theoretical reasons due to their

* Corresponding author at: Centro de Investigación y de Estudios Avanzados del IPN, Depto. de Física, Av. IPN 2508, Distrito Federal, C.P. 07360, México D.F., Mexico.
E-mail address: necastillo@yahoo.com (N. Castillo).

0925-8388/$ – see front matter © 2009 Elsevier B.V. All rights reserved.
doi:10.1016/j.jallcom.2009.11.161

Table 1
Chemical Composition of nanoparticles Pd_x–$Pt_{(1-x)}$.

Bimetallic sample	Composition (wt%)			
	Precursors		EDS	
	Pt	Pd	Pt	Pd
S1 Pt_{20}–Pd_{80}/TiO_2	20	80	20.10	79.9
S2 Pt_{50}–Pd_{50}/TiO_2	50	50	50.64	49.36
S3 Pt_{80}–Pd_{20}/TiO_2	80	20	80.03	19.97

mass forms that offer superior activity, higher selectivity and higher poison resistance than monometallic Pt or Pd catalyst in skeletal isomerization [35,36]. These bimetallic systems have reported a high tolerance to sulfide catalysts in hydrogenation of aromatics. Therefore these materials in the form of nanoparticles have a broad application and they are very attractive in the design of better catalysts and materials. In order to develop such systems, it is important to understand the nanoparticles formation mechanisms and the parameters that influence their growth on the method used in the synthesis to relate to catalytic activity.

2. Experimental

Bimetallic nanoparticles were prepared by impregnation on TiO_2 (Degussa P25). Different atomic concentrations of Pd and Pt were used to obtain three samples, 1 wt% of total metal content was supported. The metal precursor and TiO_2 were dispersed and stirred in aqueous solution for 6 h at room temperature. Then, solids were separated by evaporation. The solids were then dried at 353 K overnight, before thermal treatment under hydrogen flow at 673 K for 4 h. Chloroplatinic acid (H_2PtCl_6) and palladium chloride ($PdCl_4$) were used as metal precursors. Table 1 presents the chemical composition of different bimetallic Pt_x–$Pd_{(1-x)}$ alloys, where x represents the ratio between Pt and Pd content.

The materials were characterized by X-ray diffraction (XRD), N_2 sorption, transmission electron microscopy (TEM). XRD patterns were recorded on a Siemens D5000 instrument using Cu Kα radiation (λ = 1.54 Å) at 35 kV and 25 mA. N_2 sorption experiments at 77 K were carried out with a Micromeritics ASAP 2000 instrument, and specific surface areas were calculated using the BET method. The metal particles were examined by transmission electron microscopy (TEM) using a JEOL 4000 microscope (λ = 0.17 nm at 400 keV).

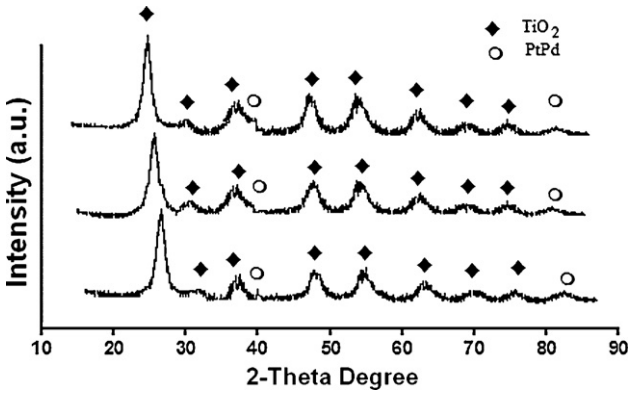

Fig. 1. X-ray diffraction patterns of Pt_x–$Pd_{(1-x)}$ bimetallic nanoparticles supported on anatase TiO_2.

The catalytic tests in the cyclo-hexene reaction were performed under atmospheric pressure in a microflow fixed-bed reactor (6 mm i.d.) using 100 mg of catalyst (grain size: 63–125 μm) at 523 K. Prior to any measurements, the catalysts were submitted to in situ heated in N_2 at 473 K for 2 h (ramp: 6 K/min). Cyclo-hexene was fed by bubbling N_2 through a saturator at 298 K. The reactant was then passed through the catalyst at 523 K and the effluent sampled at regular time intervals of 20 min for analyzing with a gas chromatograph FID-GC with a capillary column of OV-101-(PIONA) at 523 K. Product stream at the reactor exit was collected in an ice cooled trap every 5 min. The following parameters were determined to evaluate the catalytic properties:

$$\text{cyclo-hexene conversion} = \frac{\text{cyclo-hexene}_{in} - \text{cyclo-hexene}_{out}}{\text{cyclo-hexene}_{in}} \times 100$$

3. Results and discussion

X-ray diffraction peaks, corresponding to a face centered cubic (FCC) structure, can be observed in Fig. 1. Lattice parameters (a), calculated by XRD, were 0.389, 0.390 and 0.391 nm for S1, S2 and S3 samples, respectively (see Table 2 and Fig. 1). While TiO_2

Table 2
Specific surface area, structure, lattice parameter, diameter and conversion to methyl-cyclopentene of the bimetallic nanoparticles.

Bimetallic nanoparticle Pt_x–Pd_{1-x}	Structure Pt_x–Pd_{1-x}/TiO_2 by XRD	Lattice parameter Pt_x–Pd_{1-x} (nm)	Bimetallic nanoparticles Pt_x–Pd_{1-x} diameter (nm)	BET ($m^2\ g^{-1}$)	Conversion (%)
S1 Pt_{20}–Pd_{80}/TiO_2	FCC/tetragonal	a = 0.389	6.1	19.66	86
S2 Pt_{50}–Pd_{50}/TiO_2	FCC/tetragonal	a = 0.390	5.2	21.39	95
S3 Pt_{80}–Pd_{20}/TiO_2	FCC/tetragonal	a = 0.391	4.2	29.40	98

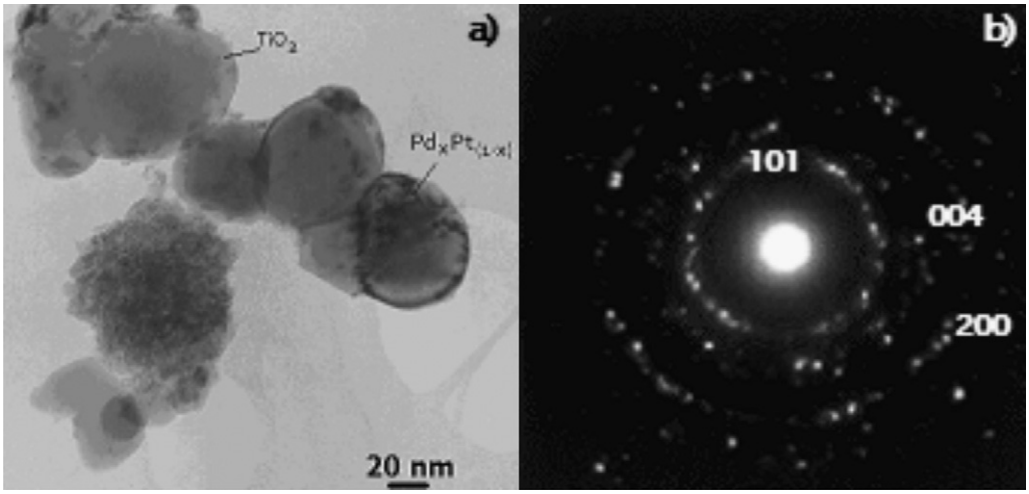

Fig. 2. TEM of Pt_x–Pd_{1-x} bimetallic nanoparticles supported on TiO_2. Morphology, phase and crystallographic orientation, selected area electron diffraction (SAED) S1.

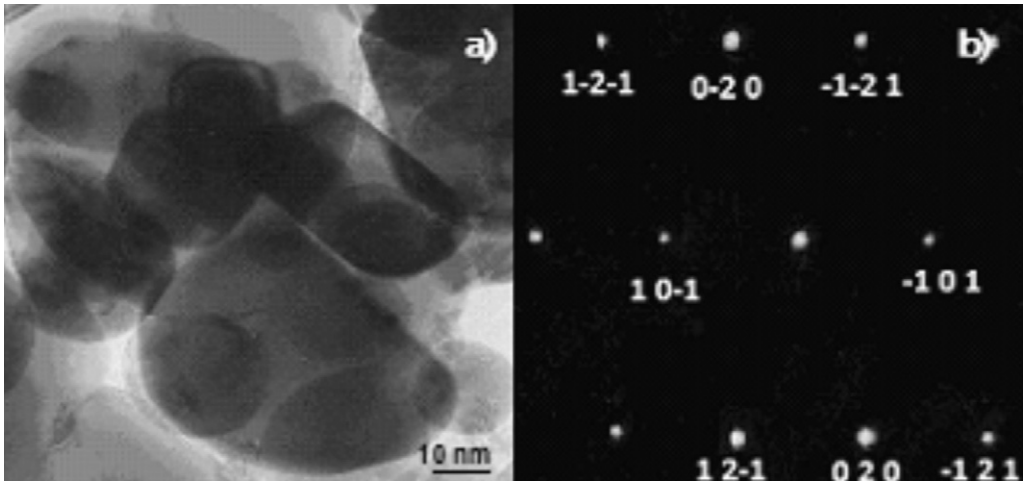

Fig. 3. TEM of Pt_x–Pd_{1-x} bimetallic nanoparticles supported on TiO_2. Morphology, phase and crystallographic orientation, selected area electron diffraction (SAED) S2.

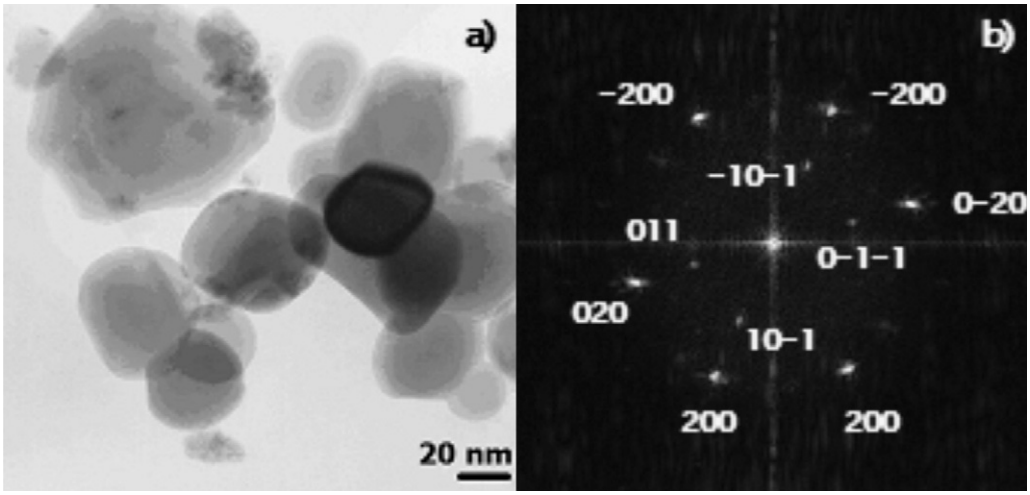

Fig. 4. TEM of Pt_x–Pd_{1-x} bimetallic nanoparticles supported on TiO_2. Morphology, phase and crystallographic orientation, selected area electron diffraction (SAED) S3.

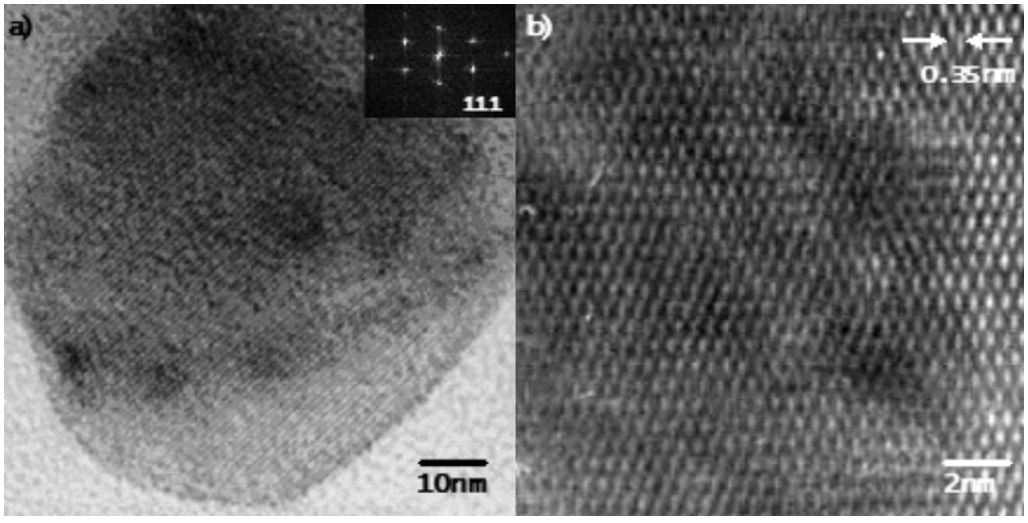

Fig. 5. (a) HREM image of platinum–palladium bimetallic nanoparticle supported on TiO_2, and patter electron diffraction (b) platinum–palladium interaction with TiO_2, strong metal support interaction (SMSI).

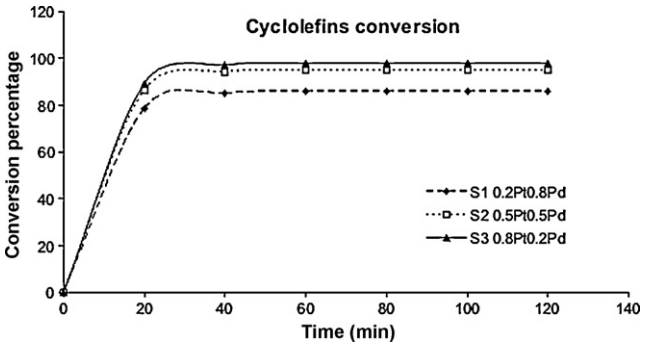

Fig. 6. Conversion vs time of cyclo-hexene isomerization reaction.

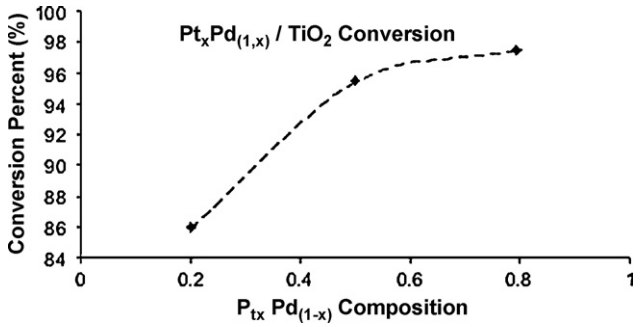

Fig. 7. Conversion vs Pt–Pd composition of cyclo-hexene isomerization reaction.

support (anatase-like structure), presents a tetragonal structure (a = 0.37842 nm, b = 0.37842 nm and c = 0.95146 nm).

Bimetallic Pt_x–$Pd_{(1-x)}$ nanoparticles studied by HRTEM are shown in Figs. 2–4. Nanoparticles were directly observed using the bright field technique. In Fig. 2, nanoparticles, with sizes lower than 10 nm, were observed on TiO_2 support, support diameter was higher than 50 nm. In Fig. 2b, a selected area diffraction pattern with rings of sample S1 was observed and related to a polycrystalline FCC structure. In this case, structure corresponds to a Pt–Pd solid solution with lattice parameter a = 0.3891 nm in good agreement with XRD results.

In order to study small areas of samples, in Figs. 3 and 4, digital diffractograms of samples S2 and S3 were formed by Fast Fourier Transform (FTT) with CRISP program. Using this program, it was also measured interplanar distances in order to establish local structure and lattice parameters. In all cases, PtPd bimetallic nanoparticles presented a FCC structure while TiO_2 presented tetragonal structure and lattice parameters are comparables with those obtained by XRD. It was also observed a relation between diameter sizes and composition: lattice parameter increases when Pt content is higher (see Table 2). The average size of PtPd synthesized nanoparticles ranged from 4 to 6 nm. The electron interactions, with heavy atoms, are stronger than light atoms. If the thickness samples are homogeneous, areas in which heavy atoms are concentrated appear with darker contrast than such with light atoms (mass contrast), Pt (molecular weight = 195.08 uma) is heavier than Pd (molecular weight = 106.42 uma). Thus, it could be possible that brighter points could be associated to Pd and points with low intensity are those of Pt. In this way, it is proposing a weighting factor. Bimetallic nanoparticles were observed by HREM (see Fig. 5). Different zones were studied by FFT in order to establish their structure. In all cases, bimetallic systems present FCC structure, they have (1 1 1) plane, where the function of intensity pattern points presented have different distributions of the metal nanoparticles. FFT images show the intensities of points, associated with the inverse of density [37].

In Table 1, chemical compositions of nanoparticles were evaluated by EDS in the HRTEM. The observed compositions of samples by this technique are in good agreement with those expected by chemical composition in bimetallic nanoparticles production.

Fig. 6 shows cyclo-olefin conversion as a function of time. It should be remarked that in the course of the reaction, it could observe that main product was methyl-cyclo-pentene taking into account the peak areas of chromatograms. On the other hand, Fig. 7 shows cyclo-hexene conversion as a function of chemical composition of the solids. It is clear that all catalysts show high activity (from 86 to 98%), however, S3 sample shows the highest conversion rate to methyl-cyclo-pentene in the isomerization of cyclo-hexene (Fig. 7). These results could be associated to the Pt/Pd atomic ratio, as well as physicochemical properties of TiO_2 support [2].

In according to the platinum composition in the samples, that increase from 20 to 80%, corresponding to samples S1 to S3, respectively, bimetallic nanoparticles improve the catalytic conversion of cyclo-hexene, and they are attributed to the surface properties of these bimetallic particles. However, the arrangement and concentration of platinum and palladium are important because of the conversion rate. Moreover, the effect of the metal ratios determines the activity towards methyl-cyclo-pentene. Even though, total metal concentration was constant (1 wt%), the variation of Pt/Pd atomic ratio provides an important effect on catalytic activity. Is should be noted that growth of particles on the surface of support, exposed to the reagent, has a major effect on the conversion, due to olefins isomerization is a unimolecular reaction and it should occur on all sites, including isolated sites. The higher isomerization conversion rate of the catalyst with the lowest unit cell size may be attributed to planes PtPd (1 1 1) and (1 0 0).

In Table 2, BET surface area results are shown for samples S1, S2 and S3, as well as bimetallic nanoparticle composition, crystalline structure, diameter sizes, measures by TEM techniques, and conversion percent. According to results, while platinum content in particles is higher, surface area increase, however it is well known that a variation from 20 to 29 m^2/g it is not significant due to error % of the measures. On the other hand, particle diameter size is lower and lattice parameter (a) increase when Pt content increases. Analyzing atomic ratio and lattice parameters of Pt and Pd, it is possible to establish that sample a big amount of palladium atoms are mainly distributed outside of the particle for S1 sample, because alloy lattice parameter is near to Pd lattice parameter, a = 0.38903 nm, while platinum atoms are mainly in particle surface for S3 sample (Pt lattice parameter a = 0.39236 nm).

4. Conclusions

Cyclo-hexene isomerization reaction was carried out to improve the catalytic activity of a series of bimetallic PtPd supported materials. PtPd bimetallic nanoparticles presented a FCC structure while TiO_2 presented tetragonal structure. Highs conversion rates were obtained for all solids and main product was methyl-cyclo-pentene and the sample containing 0.8 wt% of platinum and 0.2 wt% of palladium shows the highest catalytic conversion in cyclo-olefin reaction.

Based on catalytic and characterization results, it could be attributed that isomers production is performed on PtPd (1 1 1)/TiO_2 and PtPd (1 0 0)/TiO_2. Notwithstanding low surface area of TiO_2 (20–29 m^2/g), this support demonstrated to be active to the cyclo-hexene isomerization reaction. Finally, when the platinum content increased from 0.2 to 0.8 wt%, the average size of PtPd nanoparticles decreased, while cell parameter in the alloy Pt–Pd increase. Growth of particles on the surface of support, exposed to the reagent, has a major effect on the conversion because of cyclo-olefin reaction is a structure-sensitive reaction.

Acknowledgements

Authors wish to thank Luis Rendon and Angel Flores from IFUNAM for technical assistance in Electron Microscopy. Also wish to thank to CONACYT for scholarship 154071, CONACYT 61597 and SIP 20082453, 20090868 projects for financial support.

References

[1] S. Koutsopoulos, T. Johannessen, K.M. Eriksen, R. Fehrmann, J. Catal. 238 (2006) 206–2132.
[2] U. Diebold, Surf. Sci. Rep. 48 (2003) 53–229.
[3] J.M. Hernann, J. Disdier, P. Pichat, A. Fernandez, A.G. Felipe, G. Munuera, C. Leclercq, J. Catal. 132 (1991) 490–497.
[4] J.L. Rousset, F.J.C.S. Aires, F. Bornette, M. Cattenot, M. Pellarin, L. Stievano, A.J. Renouprez, Appl. Surf. Sci. 164 (2000) 163–168.
[5] N. Toshima, Pure Appl. Chem. 72 (2000) 317–325.
[6] K. Thomas, C. Binet, T. Chevreau, D. Cornet, J.P. Wilson, J. Catal. 212 (2002) 63–75.
[7] N. Toshima, Y. Shiraishi, A. Shiotsuki, D. Ikenaga, Y. Wang, Eur. Phys. J. D 16 (2001) 209–212.
[8] W. Tu, S. Cao, L. Yang, W. Wang, Chem. Eng. J. 143 (2008) 244–248.
[9] T. Fujikawa, K. Tsuji, H. Mizuguchi, H. Godo, K. Idei, K. Usui, Catal. Lett. 63 (1999) 27–33.
[10] W. Qian, H. Shirai, M. Ifuku, A.i. Ishihara, T. Kabe, Energy Fuels 14 (2000) 1205–1211.
[11] Z. Baoquan, G. Ruijie, L. Xiufeng, Appl. Surf. Sci. 254 (2008) 5394–5398.
[12] M. Arenz, V. Stamenkovic, T.J. Schmidt, K. Wandelt, P.N. Rossa, N.M. Markovica, Phys. Chem. Chem. Phys. 5 (2003) 4242–4251.
[13] J. Wang, P. Holt-Hindle, D. MacDonald, F.D. Thomas, A. Chen, Electrochim. Acta 53 (2008) 6944–6948.
[14] K. Persson, J. Kjell, G.S. Jaras, J. Catal. 245 (2007) 401–414.
[15] A. Niquille-Rothlisberger, R. Prins, J. Catal. 242 (2006) 207–216.
[16] K. Persson, A. Ersson, K. Jansson, G.J.L. Fierro, S.G. Jaras, J. Catal. 243 (2006) 14–24.
[17] L. Qingsheng, J.C. Bauer, E.S. Raymond, H.L. Jack, Appl. Catal. A 339 (2008) 130–136.
[18] A.E. Cordero-Borboa, E. Sterling-Black, A. Gómez-Cortés, A. Vázquez-Zavala, Appl. Surf. Sci. 220 (2003) 169–174.
[19] G. Cocco, G. Carturan, S. Enzo, L. Schiffini, J. Catal. 85 (1984) 405–414.
[20] O. Outiki, E. Lamy, J. Barbier, Catal. Lett. 18 (1981) 127–132.
[21] C. Massen, T.V. Mortimer-Jones, R.L. Johnston, J. Chem. Soc. Dalton Trans. (2002) 4375–4388.
[22] M. Feng, R.J. Puddephatt, Chem. Mater. 15 (2003) 2696–2698.
[23] K.K. Bando, T. Matsui, Y. Ichihashi, K. Sato, T. Tanaka, M. Imamura, N. Matsubayashi, Y. Yoshimura, Phys. Scripta 3 (2005) 828–830.
[24] C.A. Jan, T.B. Lin, J.R. Chang, Ind. Eng. Chem. Res. 35 (1996) 3893–3898.
[25] R.M. Navarro, B. Pawelec, J.M. Trejo, R. Mariscal, J.L. Fierro, J. Catal. 189 (2000) 184–194.
[26] H. Yasuda, Y. Yoshimur, Catal. Lett. 46 (1997) 43–48.
[27] H. Yasuda, N. Matsubayashi, T. Sato, Y. Yoshimura, Catal. Lett. 54 (1998) 23–27.
[28] C. Song, A.D. Schmitz, Energy Fuels 11 (1997) 656–661.
[29] N. Gyorffya, M.B.L. Tóthb, J. Ocskóc, U. Wildd, R. Schlögld, D. Teschnera, Z. Paála, J. Mol. Catal. A 238 (2005) 102–110.
[30] A. Morlang, U. Neuhausen, K.V. Klementiev, F.W. Schu¨tze, G. Miehe, H. Fuess, E.S. Lox, A. Morlang, U. Neuhausen, K.V. Klementiev, F.-W. Schütze, G. Miehe, H. Fuess, E.S. Lox, Appl. Catal. B: Environ. 60 (2005) 191–199.
[31] T. Fujikawa, K. Idei, T. Ebihara, H. Mizuguchi, K. Usui, Appl. Catal. A 192 (2001) 71–77.
[32] T. Fujikawa, K. Idei, K. Usui, J. Jpn. Petrol. Inst. 42 (1999) 271.
[33] R. Morales, F. Zaera, J. Phys. Chem. C 111 (2007) 18367–18375.
[34] S.R. Calvo, P.B. Balbuena, Surf. Sci. 601 (2007) 4786–4792.
[35] A. Bernas, N. Kumar, P. Mäki-Arvela, N.V. Kul'kova, B. Holmbom, T. Salmi, D.Y. Murzin, J.A.d.l. Reyes, Appl. Catal. A 245 (2003) 257–275.
[36] I.R. Galindo, J.A.d.l. Reyes, Fuel Process. Technol. 88 (2007) 859–863.
[37] D.B. Williams, C.B. Carter, Transmission Electron Microscopy, Plenum Press, New York, 1996.